Multiband coupling and electronic structure of $(InAs)_n/(GaSb)_n$ superlattices

L.-W. Wang, S.-H. Wei, T. Mattila, and A. Zunger
National Renewable Energy Laboratory, Golden, Colorado 80401

I. Vurgaftman and J. R. Meyer
Naval Research Laboratory, Washington DC 20375

(Received 12 April 1999)

The electronic structure of abrupt $(InAs)_n/(GaSb)_n$ superlattices is calculated using a plane wave pseudopotential method and the more approximate eight band $\mathbf{k}\cdot\mathbf{p}$ method. The $\mathbf{k}\cdot\mathbf{p}$ parameters are extracted from the pseudopotential band structures of the zinc-blende constituents near the Γ point. We find, in general, good agreement between pseudopotential results and $\mathbf{k}\cdot\mathbf{p}$ results, except as follows. (1) The eight band $\mathbf{k}\cdot\mathbf{p}$ significantly underestimates the electron confinement energies for $n\leqslant 20$. (2) While the pseudopotential calculation exhibits (a) a zone center electron-heavy hole coupling manifested by band anticrossing at $n=28$, and (b) a light hole–heavy hole coupling and anticrossing around $n=13$, these features are absent in the $\mathbf{k}\cdot\mathbf{p}$ model. (3) As $\mathbf{k}\cdot\mathbf{p}$ misses atomistic features, it does not distinguish the C_{2v} symmetry of a superlattice with no-common-atom such as InAs/GaSb from the D_{2d} symmetry of a superlattice that has a common atom, e.g., InAs/GaAs. Consequently, $\mathbf{k}\cdot\mathbf{p}$ lacks the strong in-plane polarization anisotropy of the interband transition evident in the pseudopotential calculation. Since the pseudopotential band gap is larger than the $\mathbf{k}\cdot\mathbf{p}$ values, and most experimental band gaps are even smaller than the $\mathbf{k}\cdot\mathbf{p}$ band gap, we conclude that to understand the experimental results one must consider physical mechanisms beyond what is included here (e.g., interdiffusing, rough interfaces, and internal electric fields), rather than readjust the $\mathbf{k}\cdot\mathbf{p}$ parameters. [S0163-1829(99)07531-1]

I. INTRODUCTION

$(InAs)_n/(GaSb)_m$ forms an interesting superlattice and quantum-well system, because for large periods $(n,m)\to\infty$ this heterojunction has a *negative* band gap (the InAs conduction band minimum is $\sim$160 meV below the GaSb valence band maximum), while for smaller periods, quantum confinement of InAs electrons and GaSb holes leads to finite, positive band gaps $E_g(n,m)$ of up to $\sim+400$ meV. Thus, by selecting (n,m), one can construct lasers and detectors at technologically useful, tunable IR wavelengths.[1,2] The design of such structures relies on the accurate modeling of $E_g(n,m)$. This has been largely done in the past via the $\mathbf{k}\cdot\mathbf{p}$ effective mass approximation.[3–5] Application of the $\mathbf{k}\cdot\mathbf{p}$ method to superlattices involves the following approximations:

(i) In the $\mathbf{k}\cdot\mathbf{p}$ method the superlattice states are described via a linear combination of just a few zone-center (Γ) bulk-periodic states of the underlying zinc-blende constituents. In the conventional eight band $\mathbf{k}\cdot\mathbf{p}$ model, one uses as basis the sixfold zinc-blende *p*-like valence band maximum (VBM) states $\Gamma_{7v}+\Gamma_{8v}$ and the twofold zinc-blende *s*-like conduction band minimum (CBM) states Γ_{6c}. It has previously been recognized[6–8] that one can quantify the effect of this $\mathbf{k}\cdot\mathbf{p}$ basis set truncation on nanostructures by considering its performance in describing the dispersion relation of the bulk zinc-blende constituents themselves. One finds[6–8] that while the $\mathbf{k}\cdot\mathbf{p}$ method reproduces, by construction, the correct energies at the Brillouin zone center $\mathbf{k}_0=0$, the wave vector distance $\mathbf{k}_c-\mathbf{k}_0$, outside which significant errors in the bulk dispersion relationship can be seen, is sometimes surprisingly small (see Ref. 6 for GaAs and AlAs, Ref. 7 for InP and CdSe). An extreme case is the zinc-blende X_{1c} state, where the eight-band $\mathbf{k}\cdot\mathbf{p}$ method overestimates its position by[6] 9 eV in GaSb, 5 eV in InAs and 25 eV in GaAs. Many more than 8 bulk bands at Γ are needed to reduce the error to $\sim$10–20 meV. The basic reason for this is[6] that just a few zinc-blende Bloch states drawn from the Γ-point are not enough to describe the off-Γ (i.e, $k>k_c$) states. Thus, the few band $\mathbf{k}\cdot\mathbf{p}$ method is expected to work only for superlattices with sufficiently large periods (n,m), where the band-edge wave functions are made primarily from low-momentum bulk Bloch states with $k\ll k_c$. However, technologically useful IR wavelengths in $(InAs)_n/(GaSb)_m$ typically require rather small periods (n,m) of 4–12 ML.

(ii) In the $\mathbf{k}\cdot\mathbf{p}$ method the Γ Bloch functions of the constituents are implicitly assumed to be equal, e.g., $u_\Gamma(\text{GaAs})=u_\Gamma(\text{InAs})$. This neglects the chemical uniqueness of the wave functions of the heterojunction partners. This approximation $u_\Gamma(\text{AB})=u_\Gamma(\text{CD})$ then implies that a carrier traveling from material AB to CD sees, in the $\mathbf{k}\cdot\mathbf{p}$ method, a potential barrier that equals the AB/CD band offset, while in reality, if $u_\Gamma(\text{AB})\neq u_\Gamma(\text{CD})$ there is an additional effective potential barrier, as discussed by Burt.[9]

(iii) The $\mathbf{k}\cdot\mathbf{p}$ fails to recognize atomistic details. It thus treats a C_{2v}-symmetric no-common-atom superlattice[10] such as $(InAs)_n/(GaSb)_m$ as if it was a D_{2d}-symmetric, common-atom superlattice such as $(InAs)_n/(GaAs)_m$ or $(InSb)_n/(GaSb)_m$. In a common-atom superlattice such as $(InSb)_n/(GaSb)_m$, the two interfaces are symmetry equivalent, i.e., the one with [110] In-Sb bonds plus $[\bar{1}10]$ Ga-Sb bonds is equivalent to the other one with $[\bar{1}10]$ In-Sb bonds plus [110] Ga-Sb bonds. As a result, in this D_{2d}-symmetry (eight point group operations), the two in-plane directions [110] and $[\bar{1}10]$ are equivalent, and all states are invariant under a $(x,y,z)\to(y,-x,-z)$ operation. By contrast, in a no-common-atom superlattice such as $(InAs)_n/(GaSb)_m$, the two interfaces have chemically distinct bonds: one has [110] Ga-Sb and $[\bar{1}10]$ In-Sb bonds, while the second inter-

TABLE I. Band parameters extracted from the pseudopotential (PP) band structure and the target band parameters at $T=0$ K we aim to fit. The bulk InAs and GaSb assume their natural lattice constants $a=6.050$ and $a=6.082$ Å, respectively. The parameters γ_1, γ_2, and γ_3 are the Luttinger (i.e., 6 band) $\mathbf{k}\cdot\mathbf{p}$ parameters. Δ_0 is the spin-orbit splitting, E_p is the s-p mixing parameter, and m^* are the effective masses. $\Delta E_{\mathrm{VBO}} \equiv E_{\mathrm{VBM}}(\mathrm{InAs}) - E_{\mathrm{VBM}}(\mathrm{GaSb})$ is the valence band offset. a_g, a_v, and a_c are the hydrostatic deformation potentials for band gap, valence band, conduction band, respectively, and b is the biaxial deformation potential of the valence band. The ''target values'' shown in the first eleven lines represent conventional bulk parameters used in the literature, which we have fitted in the present PP work. The ''target values'' for the quantities in the last four lines are derived from first-principles LDA calculations. They differ from values often used in the literature given here in parentheses and are not fitted explicitly.

	InAs		GaSb	
	Current PP fit	Target value	Current PP fit	Target value
γ_1	19.90	19.67	11.99	11.80
γ_2	8.57	8.37	4.27	4.03
γ_3	9.48	9.29	5.36	5.26
E_g(eV)	0.401	0.410	0.807	0.811
Δ_0(eV)	0.400	0.390	0.911	0.752
E_p(eV)	21.14	19.90	22.24	22.60
ΔE_{VBO}			−0.553	−0.540
m_e^*	0.022	0.024	0.042	0.041
$m_{hh}^*(100)$	0.361	0.341	0.290	0.267
$m_{hh}^*(111)$	0.867	0.917	0.781	0.781
$m_{lh}^*(100)$	0.027	0.028	0.049	0.050
a_g	−7.71	−5.66 (−6.08)	−2.59	−8.01 (−7.64)
a_v	1.43	−1.00 (1.00)	3.39	−1.32 (0.79)
a_c	−6.28	−6.66 (−5.08)	0.81	−9.33 (−6.85)
b	−2.57	−1.67 (−1.80)	−2.15	−1.98 (2.00)

face has $[\bar{1}10]$ Ga-As bonds and [110] In-As bonds. As a result, the two in-plane directions [110] and $[\bar{1}10]$ are inequivalent,[11–14] and the symmetry is reduced to C_{2v} (four point group operations). Similarly, the $\mathbf{k}\cdot\mathbf{p}$ does not recognize the proper odd-even symmetry of a film made of an odd or even number of monolayers,[15] or the correct C_{2v} symmetry of a self-assembled InAs/GaAs pyramidal dot.[16] The existence of a lower, C_{2v} symmetry in InAs/GaSb superlattices than the one (D_{2d}) assumed in standard $\mathbf{k}\cdot\mathbf{p}$ method has several consequences. (a) The two interfaces have different strain and different band offsets.[17] (b) A built-in electric field is now symmetry allowed,[17] even though we are dealing with a nonpiezoelectric (001) oriented superlattice. (c) Interband coupling can be enhanced. Indeed, the lower the symmetry of a structure, the more likely that its states have an equal symmetry representation. (In the extreme case of structures with no symmetry, all states have the same Γ_1 symmetry representation.) Since states with equal symmetry representations can interact, mix, and ''anticross,'' a lowering of the structural symmetry can enhance such interband coupling. (d) Optical polarization anisotropy is allowed for light polarized along [110] and $[\bar{1}10]$ directions. By approximating the actual C_{2v} symmetry by a higher, D_{2d} symmetry, the conventional $\mathbf{k}\cdot\mathbf{p}$ misses these effects. This effect was seen experimentally in InP/InGaAs superlattices.[13]

In this paper, we attempt to establish both the ''$\mathbf{k}\cdot\mathbf{p}$ zinc-blende errors'' (i) and the ''$\mathbf{k}\cdot\mathbf{p}$ superlattice errors,'' (ii) and (iii), by comparing the predictions of a fully atomistic multiband pseudopotential treatment of $(\mathrm{InAs})_n/(\mathrm{GaSb})_m$ with those of an eight-band $\mathbf{k}\cdot\mathbf{p}$ method, *whose parameters are drawn precisely from the same pseudopotential bulk band structures*. In other words, we first accurately parametrize the full-zone band structures of bulk GaSb and bulk InAs (at a few pressures) via pseudopotentials V_{GaSb} and V_{InAs}. Once determined, those pseudopotentials are used for calculating the InAs/GaSb superlattices via (a) a direct pseudopotential plane-wave approach and (b) an eight-band $\mathbf{k}\cdot\mathbf{p}$ approach with parameters drawn from V_{GaSb} and V_{InAs}. We deliberately neglect in the pseudopotential calculation the effect of internal electric fields, which are also lacking in $\mathbf{k}\cdot\mathbf{p}$. Thus, the two approaches share the same zinc-blende band structures at Γ, the same deformation potentials and the same GaSb-InAs band offsets. The differences in the ensuing electronic structure obtained by the $\mathbf{k}\cdot\mathbf{p}$ vs the pseudopotential method stems then entirely from the fact that $\mathbf{k}\cdot\mathbf{p}$ uses a limited eight band representation, while the pseudopotential uses a complete basis set that resolves the atomistic details. Such a comparison between a more complete theory with a less complete thery is useful for understanding possible fundamental deficiencies in the $\mathbf{k}\cdot\mathbf{p}$ theory, deficiencies that are otherwise obscured by readjustment of the $\mathbf{k}\cdot\mathbf{p}$ parameters to directly fit the experimental results on the nanostructure.

Here it is important to emphasize two points.

(a) Previous comparisons of pseudopotential calculations with $\mathbf{k}\cdot\mathbf{p}$ for InAs/GaAs[18,19] have not constrained the parameters of the two methods (e.g., Table I) to be equivalent, and so the results have not necessarily reflected only the difference in approximations, but could also have reflected different, uncontrolled inputs.

(b) In our methodology the $\mathbf{k}\cdot\mathbf{p}$ parameters are viewed as fixed constants not as adjustable parameters. Once determined from the bulk band structures (drawn from well-established experiments and state-of-the-art *ab initio* calculations, see below) they have not been readjusted to fit the superlattice experimental data, or the superlattice pseudopotential calculation. Indeed, in $\mathbf{k}\cdot\mathbf{p}$ theory the input parameters are fundamentally bulk quantities, not properties of the nanostructures themselves.

II. METHOD OF CALCULATION

We first determine screened pseudopotentials $\{v_\alpha(q)\}$ as a function of momentum q for $\alpha=$ Ga, In, As, Sb, using them to calculate the bulk band structures of GaSb and InAs from which we find the $\mathbf{k}\cdot\mathbf{p}$ band parameters shown in Table I. These parameters are then used in an eight-band $\mathbf{k}\cdot\mathbf{p}$ model[4] to calculate the superlattice states. Separately, the pseudopotentials $\{v_\alpha(q)\}$ are used to *directly* calculate the electronic structure of the superlattice, using a plane wave basis[20] whose cutoff is identical to that used in constructing the pseudopotentials.

The single particle pseudopotential Schrödinger equation for either the bulk solids or the superlattice is

$$\left\{-\frac{\beta}{2}\nabla^2+\sum_{n\alpha}\hat{v}_\alpha(\mathbf{r}-\mathbf{R}_{n\alpha})\right\}\psi_i(\mathbf{r})=\epsilon_i\,\psi_i(\mathbf{r}). \qquad (1)$$

Here $\mathbf{R}_{n\alpha}$ denotes the positions of the nth atom of type α, determined from the strain minimization *via* Keating's valence force field model.[21] The distinction between bulk zinc-blende solids and superlattices in Eq. (1) is entirely due to the different atomic positions $\{\mathbf{R}_{n\alpha}\}$. Since Eq. (1) is solved but once (i.e., self-consistency is not attempted), it is important to make the screened (empirical) pseudopotentials $\{\hat{v}_\alpha\}$ as accurate as possible, at the outset. Thus, $\hat{v}_\alpha$ contains a local part and a nonlocal spin-orbit interaction part. Due to the spin-orbit coupling, the wave function $\psi(\mathbf{r})$ is complex and has both spin up and spin down components. The spin-orbit nonlocal potential is calculated using a small box implementation as described in Ref. 22. The local part of the potential has an analytical form in reciprocal space q:

$$v_\alpha(q)=[1+\gamma_\alpha \mathrm{Tr}\,\epsilon(\mathbf{R}_{n\alpha})]\frac{a_{0\alpha}(q^2-a_{1\alpha})}{a_{2\alpha}e^{a_{3\alpha}q^2}-1}. \qquad (2)$$

Here, the prefactor in square brackets depends on the local strain $\mathrm{Tr}\,\epsilon(\mathbf{R}_{n\alpha})$ of atom $\mathbf{R}_{n\alpha}$. This introduces a local environmental dependence of the screened pseudopotential, mimicking the situation in self-consistent calculations (see Ref. 23 for more details about this local strain dependent term). In Eq. (1), we have also scaled the kinetic energy ($\beta\neq1$), partly to represent the effects of the ignored quasiparticle nonlocal self-energy term.[24] In practice, the kinetic energy scaling is needed to fit both the effective masses and energy gaps. In this calculation, we have used $\beta=1.205$. The superlattices are assumed to have a lateral lattice constant equal to the natural GaSb lattice constant, and the whole system is relaxed in the [001] direction using a Keating valence force field model.[21] The calculated c/a ratios are shown in the boxed areas in Fig. 1.

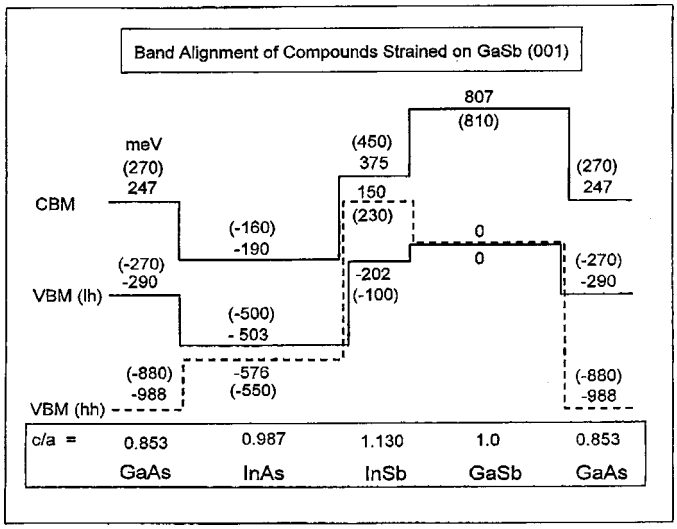

FIG. 1. Pseudopotential band alignments (in meV) of the InAs/GaSb (001) superlattices coherently matched to a GaSb substrate. The lateral lattice constant equals the GaSb natural lattice constant $a=6.082$ Å. The (001) direction lattice constants for all the compounds have been relaxed accordingly, resulting in the c/a ratio shown in the figure. Numbers in parentheses are the LDA results, corrected for the LDA band gap error.

The pseudopotential parameters $\{\gamma_\alpha, a_{0\alpha}, a_{1\alpha}, a_{2\alpha}, a_{3\alpha}\}$ of Eq. (2) are adjusted to fit the *experimentally measured* electron and hole effective masses, band gaps and spin-orbit splittings, and also the *LDA-predicted* deformation potentials and band alignments. The target values we aim to fit are given in Table I. A 5 Ry kinetic energy cutoff was used when generating the pseudopotentials. To avoid discontinuities in the calculated band structure, a smoothing function was applied near the cutoff energy[25] E_{cut}. A few comments are in order on the target data set that we fitted.

(1) An $(\mathrm{InAs})_n/(\mathrm{GaSb})_n$ superlattice with integer period n contains not only In-As and Ga-Sb intralayer bonds, but also Ga-As and In-Sb *interfacial* bonds. In the case of lattice matching to a GaSb substrate, the Ga-As (In-Sb) interfacial bonds are strongly stretched (compressed). The bottom of Fig. 1 shows the values of the tetragonal c/a ratio which result from lattice matching to GaSb. Its departure from unity represents strain effects. Notice how deformed are the GaAs and InSb layers. This strain introduces the need to compute the band offsets for highly strained materials. Specifically, the following band offsets are needed: InAs-GaSb; GaAs-InSb; InAs-InSb; and GaAs-GaSb. We have calculated all of these via LAPW-LDA, and then fitted their values via our pseudopotential. The fitted band offsets are shown in Fig. 1, and are very close to the LDA calculated results (given in Fig. 1, in parenthesis). Indeed, we find that it is necessary to carefully fit all four band offsets in the pseudopotential generation so as to avoid artificial interfacial states in the ensuing superlattices.

(2) The unstrained valence band offsets that were obtained from our first-principles calculations[26] for GaX/InX with $X=$ P, As, and Sb, are 0.11, 0.06, and -0.01 eV, respectively. They are smaller than the values 0.36, 0.25 and 0.16 eV, respectively, obtained by Van de Walle's[27] ''model solid theory.'' The discrepancies between the two sets of results are primarly due to the fact that in the first-principles

TABLE II. Parameters of the pseudopotential of Eq. (2) for InAs and GaSb. The potentials are fit to a plane-wave kinetic energy cutoff of 5 Ry.

Parameter	In	As	Ga	Sb
γ_α	0.808	0.000	−.019	0.000
$a_{0\alpha}$	139.797	23.104	544918.497	266.483
$a_{1\alpha}$	1.559	3.106	1.752	2.154
$a_{2\alpha}$	2.603	1.286	7281.008	3.003
$a_{3\alpha}$	0.433	0.362	0.907	0.877

all-electron calculation the anion *p*-cation *d* coupling is fully taken into account,[26] while this effect is missing in Van de Walle's calculation.

Table I compares the $\mathbf{k}\cdot\mathbf{p}$ band parameters extracted from our pseudopotentials with the target parameters used in the literature at $T=0$ K. We see that our band parameters pertaining to the natural lattice constants (first eleven lines) fitted very well the conventional target values. However, our fitted deformation potentials differ quite significantly from the target values derived from a recent LDA calculation,[28] especially for GaSb. But, since GaSb and InAs are nearly lattice matched, we believe that the errors in the pseudopotential deformation potentials (which are not used in the fitting procedure) will not have a significant effect on the band structures calculated for superlattices strained to the GaSb substrate. What is important here is the band alignment shown in Fig. 1, which are fitted accurately.

Our pseudopotential and $\mathbf{k}\cdot\mathbf{p}$ calculations reported in this paper are based on an identical parameter set (''current fit'' in Table I). The corresponding parameters of the employed pseudopotential [Eq. (2)] are given in Table II.

III. RESULTS

A. Bulk band structures

Figure 2 compares the pseudopotential and 8×8 $\mathbf{k}\cdot\mathbf{p}$ band structures obtained for bulk GaSb and InAs using the same zone-center parameters. We see that around the Γ point, the dispersions are the same for the pseudopotential and $\mathbf{k}\cdot\mathbf{p}$ methods. The lowest $\mathbf{k}\cdot\mathbf{p}$ conduction band is accurate out to 20% of the $\Gamma-X$ distance k_x, while the heavy hole (hh) and light hole (lh) bands of GaSb band start to deviate from the pseudopotential results at about 15% of k_x, the hh and lh bands of InAs start to deviate at about 10% of k_x.

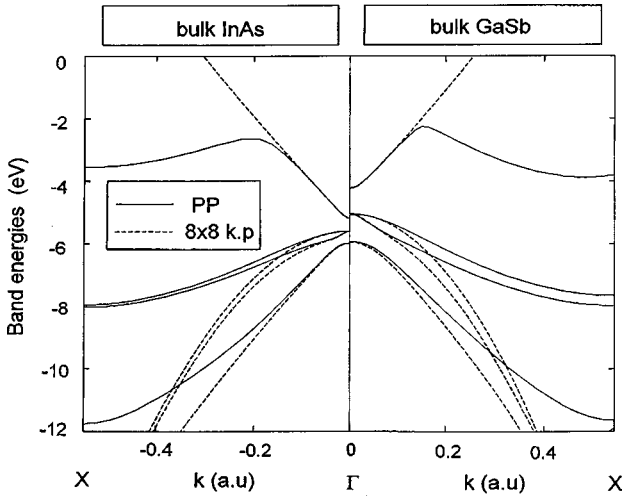

FIG. 2. Comparison of bulk band structures obtained from the pseudopotential and eight band $\mathbf{k}\cdot\mathbf{p}$ theories. The $\mathbf{k}\cdot\mathbf{p}$ results are calculated using the input parameters of Table I, which are extracted from the pseudopotential band structures near the Γ point. The valence and conduction band offsets at Γ are derived from LDA self-consistent calculations.

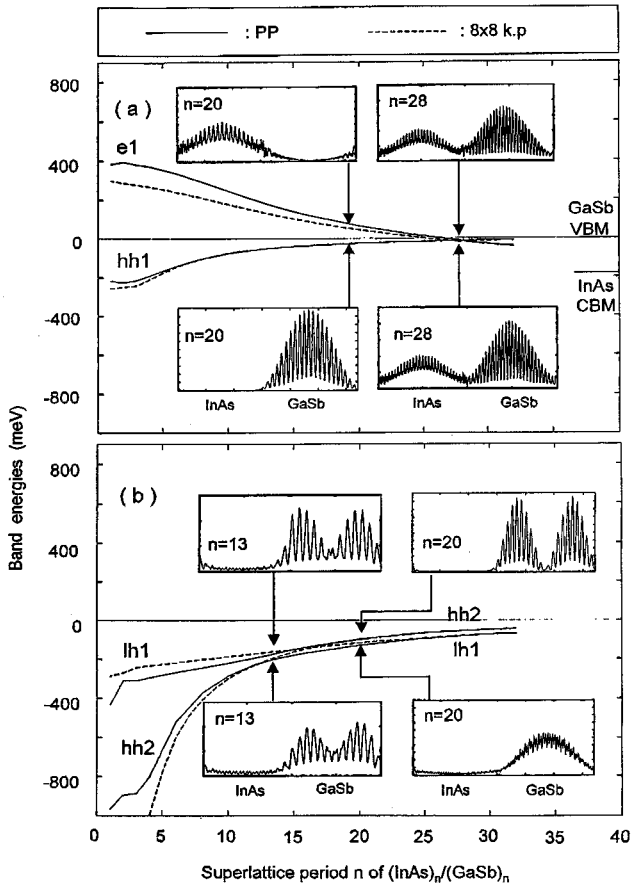

FIG. 3. Electron and hole energy levels vs the superlattice period n and the spatial dependence of pseudopotential wave functions squared (inset). The pseudopotential calculated energies (solid lines) are compared with eight band $\mathbf{k}\cdot\mathbf{p}$ energies (dashed lines). The wave functions squared are averaged over lateral directions. The interface at the center of the box is taken to have InSb bonds, and the interface at the edges of the box GaAs bonds, as in the arrangement of Fig. 1.

B. Superlattice electron and hh1 states

Figure 3(a) shows the calculated energies of the $(\mathrm{InAs})_n/(\mathrm{GaSb})_n$ superlattices as a function of layer thickness n (in ML) for the heavy-hole state hh1 and electron state e1 at $T=0$ K as obtained by the pseudopotential (solid lines) and $\mathbf{k}\cdot\mathbf{p}$ (dashed lines) methods. Asymptotically, as $n\to\infty$ the superlattice hh1 energy converges to the bulk GaSb VBM value, while the superlattice e1 energy converges to the bulk InAs CBM value, both shown on the right hand side of Fig. 3. As the period n becomes shorter, confinement moves the electron levels up and the hole levels down. The amount by which the superlattice electron (hole) energy lies

TABLE III. Energy levels of $(InAs)_n/(GaSb)_n$ (001) superlattices obtained using the pseudopotential (PP) and the $\mathbf{k}\cdot\mathbf{p}$ methods, using the input parameters from Table I. Energies are in units of meV, and zero is referenced to the valence band maximum of unstrained GaSb. For $n=1$ and 4, the ϵ_{hh2} energies are out of the range of our $\mathbf{k}\cdot\mathbf{p}$ calculation.

Period n	ϵ_e		ϵ_{hh1}		ϵ_{hh2}		ϵ_{lh}	
	PP	$\mathbf{k}\cdot\mathbf{p}$	PP	$\mathbf{k}\cdot\mathbf{p}$	PP	$\mathbf{k}\cdot\mathbf{p}$	PP	$\mathbf{k}\cdot\mathbf{p}$
1	382	297	−220	−257	−970		−432	−287
4	369	266	−194	−211	−804		−294	−235
8	291	209	−104	−104	−372	−407	−244	−203
10	244	176	−77	−76	−286	−299	−220	−187
20	62	44	−26	−26	−98	−101	−132	−123
28	−16	−20	−13	−14	−56	−56	−83	−82
32	−39	−41	−11	−11	−45	−44	−69	−70

above (below) the InAs CBM (GaSb VBM) constitutes the electron (hole) confinement energy. We see that the pseudopotential and $\mathbf{k}\cdot\mathbf{p}$ results agree not only asymptotically (as guaranteed by the identical inputs), but also for large periods ($n\geqslant 25$). At shorter periods, however, the $\mathbf{k}\cdot\mathbf{p}$ underestimates considerably the electron confinement energy and overestimates slightly the hh1 confinement energy. Table III gives some of the energy eigenvalues. We see that $\mathbf{k}\cdot\mathbf{p}$ *underestimate* electron confinement energies by 85 meV ($n=1$) to 18 meV ($n=20$), while its overestimation of hh1 energies ranges from 37 meV ($n=1$) to less than 1 meV ($n=20$). The larger electron confinement energy of the pseudopotential calculation emerges from the fact that in this calculation the Bloch functions of InAs and GaSb are allowed to differ, while in $\mathbf{k}\cdot\mathbf{p}$ they are assumed to be the same.

The insets to Fig. 3(a) illustrate the spatial variations of the wave functions squared for the electron and hole states at $n=20$ and $n=28$ as obtained by the pseudopotential calculation. The microscopic structure, induced by the Bloch function oscillation is apparent. While in $\mathbf{k}\cdot\mathbf{p}$, the electron states have pure *s* symmetry and the hh1 states have pure *p* symmetry at the zone center, the correct C_{2v} symmetry of the pseudopotential noncommon atom superlattice permits parity mixing. While the effect is smalll for $n\sim 20$ due to the limited spatial overlap of the electron and hole states, at a critical period $n_c\sim 28$ ML the electron and hole states anticross. The inset to Fig. 3(a) show the wave function squared at that point demonstrating strong mixing which is absent in the $\mathbf{k}\cdot\mathbf{p}$ calculation (i.e., $\mathbf{k}\cdot\mathbf{p}$ gives crossing, pseudopotential calculation gives anticrossing). However, the $\mathbf{k}\cdot\mathbf{p}$ calculation also give an anticrossing and interband mixing at finite in-plane $\mathbf{k}$ value.

Figure 4(a) shows the pseudopotential interband dipole transition matrix element squared $I_{ij}(\hat{\epsilon})=|\langle\psi_i|p\hat{\epsilon}|\psi_j\rangle|^2$ between the heavy hole state $i=$hh1 and the electron state $j=$e1, as a function of superlattice period *n*. We show separately the matrix element along the in-plane $\hat{\epsilon}=[110]$ polarization and $\hat{\epsilon}=[\bar{1}10]$ polarization (the superlattice is along (001) direction). Notice that the interfacial InSb and GaAs bond chains are both in the $(\bar{1}10)$ direction. For periods below $n\sim 15$, we see that the transition in the [110] direction is much stronger than that in the $(\bar{1}10)$ direction. Defining

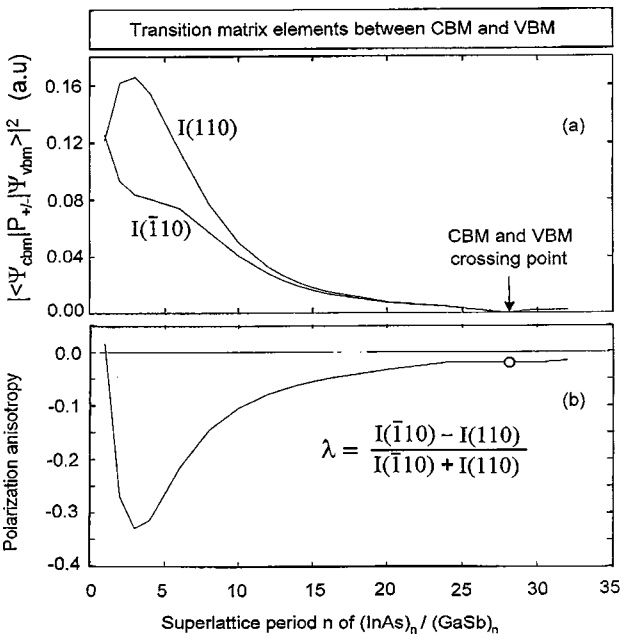

FIG. 4. Optical transition matrix elements and the anisotropy parameter λ [Eq. (3)]. See the text for definition of [110] and $[\bar{1}10]$ directions. Results are not shown for $n=28$, where the electron and hole states cross each other, and the matrix elements $I_{[110]/[\bar{1}10]}$ in Eq. (3) are very small and the anisotropy is not well defined.

$$\lambda=\frac{I[\bar{1}10]-I[110]}{I[\bar{1}10]+I[110]} \tag{3}$$

this ''giant polarization anisotropy'' is plotted in Fig. 4(b). In the conventional eight-band $\mathbf{k}\cdot\mathbf{p}$ calculation, the incorrect superlattice symmetry prohibits any such anisotropy so that $\lambda=1$. This polarization anisotropy has been observed experimentally in noncommon atom superlattices such as InAs/AlSb (Ref. 12) and InP/InGaAs (Ref. 13) (see also the calculation of Ref. 14). It would naturally diminish if the interfaces are intermixed.

C. Superlattice hh2 and lh2 states

Figure 3(b) shows the calculated energies of the second and third (zone center) superlattice hole states, which are both localized in the GaSb layer, as a function of *n*, as calculated by the pseudopotential (solid lines) and $\mathbf{k}\cdot\mathbf{p}$ (dashed line) methods. For long periods the second hole state is hh2-like while the third is lh1-like. The insets to Fig. 3(b) show the pseudopotential wave functions squared at $n=20$. The hh2 and lh1 are localized on GaSb. The hh2 state has a node (minimum) while the lh1 state has a single maximum at the center of the GaSb region. The pseudopotential and $\mathbf{k}\cdot\mathbf{p}$ results are similar for long periods. However, as the period is reduced, the second and third hole states anticross and swap their wave function characters in the pseudopotential calculations. The inset to Fig. 3(b) show the wave functions squared for the intermediate region, $n=13$, where strong lh1-hh2 mixing occurs. We see that both states have a local *minima* at the center of the GaSb part (unlike lh1), but

TABLE IV. Experimental photoluminescence energy gaps E_g(eV) at the measurement temperature T and also extrapolated to $T=0$ for equal-thickness $(InAs)_n/(GaSb)_n$ (001) superlattices.

Period n (L) in ML (Å)	$E_g(T)$	$E_g(T=0)$	Period n (L) in ML (Å)	$E_g(T)$	$E_g(T=0)$
8.5 (26)[a]	0.22–0.25	0.215–0.245	8.5 (26)[b]	0.30	
5.7 (17.5)[b]	0.36		8.9 (27)[d]	0.26	
5.9 (18)[b]	0.365		9.0 (27.5)[b]	0.265	
6.0 (18.2)[c]	0.325	0.335	9.2 (28)[b]	0.275	
6.6 (20)[b]	0.36		9.2 (28)[f]	0.33	
6.9 (21)[d]	0.32		9.8 (30)[g]	0.265	
6.9 (21)[e]	0.275	0.335	9.8 (30)[g]	0.28	
6.9 (21)[e]	0.245	0.3	12.1 (37)[d]	0.2	
8.4 (25.5)[b]	0.285		16.1 (49)[c]	0.09	0.13
			16.7 (51)[h]	0.15	
			20.3 (62)[h]	0.15	

[a]Reference 29: at $T=77$ K, InSb/or GaAs interface only.
[b]Reference 30: at $T=10$ K.
[c]Reference 31: at $T=84$ K.
[d]Reference 32: at $T=4.2$ K.
[e]Reference 33: at $T=300$ K, InSb/or GaAs interface only, grown at 450 °C.
[f]Reference 34: at $T=5$ K.
[g]Reference 35: at $T=12$ K, InSb/or GaAs interface only.
[h]Reference 36: at $T=4.8$ K.

that there is a finite amplitude there (unlike hh2 at $n=20$). Such zone center lh-hh mixing and anticrossing are absent in the $\mathbf{k}\cdot\mathbf{p}$ calculation. It is interesting to note, however, that this anticrossing does exist in $\mathbf{k}\cdot\mathbf{p}$ at off Γ in-plane wave vectors. The quantitative difference in the lh energy levels (Table III) between pseudopotential and $\mathbf{k}\cdot\mathbf{p}$ ranges from 145 meV at $n=1$ to 9 meV at $n=20$.

IV. SUMMARY

The following points emerge from the comparison of pseudopotential and $\mathbf{k}\cdot\mathbf{p}$ results.

(1) The $\mathbf{k}\cdot\mathbf{p}$ underestimates the electron confinement energy in the superlattice (Fig. 3) by $\leqslant 85$ meV even though $\mathbf{k}\cdot\mathbf{p}$ produces correct conduction band energies in bulk out to $\sim 20\%$ of the distance from Γ to X (Fig. 2). Given that the $\mathbf{k}\cdot\mathbf{p}$ and pseudopotential calculations used the same electron masses and band offsets (Table I), the $\mathbf{k}\cdot\mathbf{p}$ underestimation of electron confinement energies must originate from the treatment of the Bloch functions at the interface, as pointed out by Burt.[9]

(2) The $\mathbf{k}\cdot\mathbf{p}$ overestimates the hh1 ($\leqslant 37$ meV) and hh2 ($\leqslant 145$ meV) binding energies in the superlattice for small period n (Fig. 3), in line with its similar overly bound hh states in the bulk band structure (Fig. 2).

(3) The pseudopotential calculation indicates that while the e1 state is s-like and the hh1 state is p-like, $s-p$ parity mixing, forbidden by $\mathbf{k}\cdot\mathbf{p}$, is in fact allowed. The pseudopotential calculation shows significant e1-hh1 mixing around $n=28$ [see insets to Fig. 3(a)] which is missing in $\mathbf{k}\cdot\mathbf{p}$ at the zone center. Indeed $\mathbf{k}\cdot\mathbf{p}$ predicts a crossing of these levels, while the pseudopotential calculation shows anticrossing.

(4) In line with its assumed D_{2d} symmetry, the $\mathbf{k}\cdot\mathbf{p}$ method misses the ''giant'' (110) vs $(\bar{1}10)$ polarization anisotropy of the e1$\leftrightarrow$hh1 transition. This anisotropy results from the C_{2v} symmetry related to the existence of two chemically different interfaces in superlattices with no common atom. This effect could be introduced into the $\mathbf{k}\cdot\mathbf{p}$ formalism.[13]

(5) The pseudopotential calculation shows anticrossing and mixing at the zone center of the second and third hole states lh1 and hh2 which are missed by the $\mathbf{k}\cdot\mathbf{p}$.

It is not the purpose of this paper to discuss in detail the comparison between theory and experiment, as we have focused instead on comparing two theoretical approaches having equivalent input but different variational treatments. We see, however, in Fig. 3(a) and Table III that the variationally more complete pseudopotential calculation produces larger band gaps and smaller valence inter sub-band differences than the eight band $\mathbf{k}\cdot\mathbf{p}$ method extracted from the same underlying bulk band structures. Experimental determinations of band gaps for $n=m$ superlattices are summarized in Table IV.[29–36] While there are in some cases systematic disagreement between various experiments, we see that for short periods the measured gaps are generally *smaller* than those obtained from $\mathbf{k}\cdot\mathbf{p}$ (Table III). In Table III the band gap is given by the difference $\epsilon_e-\epsilon_{hh1}$. For $n=4$, 8, and 10, the calculated values are 0.56, 0.40, and 0.32 eV, respectively, via pseudopotentials and 0.48, 0.31, and 0.25 eV, respectively, via $\mathbf{k}\cdot\mathbf{p}$. This poses something of a dilemma: If one seeks to reduce the superlattice band gaps obtained by 8×8 $\mathbf{k}\cdot\mathbf{p}$ towards their experimental values, it is necessary to artificially *increase* the electron mass (reduce the electron confinement) and/or increase the GaSb/InAs valence band offset. These changes are not supported by the comparing data with accurate LDA calculations of band offsets. Moreover, our variationally more accurate pseudopotential calculation indicates that such improvements upon the $\mathbf{k}\cdot\mathbf{p}$ methodology lead to even larger discrepancies with the measured gaps. This suggests that adjustment of the $\mathbf{k}\cdot\mathbf{p}$ parameters is not the correct way to resolve the discrepancies.

This analysis suggests that new physical effects, thus far neglected, might need to be considered. For example, current pseudopotential and $\mathbf{k}\cdot\mathbf{p}$ calculations assume abrupt interfaces, while experiment[19,37,38] points to inter-diffused and rough interfaces[19,37] island formation[38–40] and even compositional modulation,[38] which have been shown in other short-period superlattice systems to lead to large band gap reductions. Another possibility is the internal electric field allowed by the C_{2v} symmetry of the system. To estimate the effect of internal electric field on the band gap reduction we have compared the LDA calculated band gap of $(InAs)_7InSb(GaSb)_8$ and $GaAs(InAs)_8(GaSb)_7$ with that of $(InAs)_8(GaSb)_8$. The former two structures have equivalent interfaces, and thus no electric field is induced by the interface. We find that the internal electric field reduced the band gap by about ~ 20 meV, thus, it does not appear to be a dominant effect that would explain the large discrepancy between present calculations and experimental observations.

To date, there is not enough data on intervalence energy splittings available to allow a meaningful comparison with experiment. Such experiments are called for, so that comparison with the values published here can be made.

ACKNOWLEDGMENTS

The work at NREL was supported by the U.S. Department of Energy, OER-BES, under Grant No. DE-AC36-83CH10093. Work at NRL was supported by ONR. We thank L.R. Ram-Mohan and Quantum Semiconductor Algorithms for use of the finite-element $\mathbf{k}\cdot\mathbf{p}$ software.

[1] R.M. Biefeld, A.A. Allerman, S.R. Kurtz, Mater. Sci. Eng., B **51**, 1 (1998).
[2] J.R. Meyer, L.J. Olafsen, E.H. Aifer, W.W. Bewley, C.L. Felix, I. Vurgaftman, M.J. Yang, L. Goldberg, D. Zhang, C.H. Lin, S.S. Pei, and D.H. Chow, IEE Proc.: Optoelectron. **145**, 275 (1998).
[3] M.E. Flatte, C.H. Grein, H. Ehrenreich, R.H. Miles, and H. Cruz, J. Appl. Phys. **78**, 4552 (1995).
[4] L.R. Ram-Mohan and J.R. Meyer, J. Nonlinear Opt. Phys. Mater. **4**, 191 (1995).
[5] F. Fuchs, E. Ahlswede, U. Weimar, W. Pletschen, J. Schmitz, M. Hartung, J. Jager, and F. Szmulowicz, Appl. Phys. Lett. **73**, 3760 (1998).
[6] D.M. Wood, A. Zunger, and D. Gershoni, Europhys. Lett. **33**, 383 (1996); D.M. Wood and A. Zunger, Phys. Rev. B **53**, 7949 (1996); L.-W. Wang and A. Zunger, *ibid.* **54**, 11 417 (1996).
[7] H. Fu, L.-W. Wang, and A. Zunger, Phys. Rev. B **57**, 9971 (1998).
[8] L.M. Ramaniah and S.V. Nair, Phys. Rev. B **47**, 7132 (1993).
[9] M.G. Burt, J. Phys.: Condens. Matter **4**, 6651 (1992).
[10] R.G. Dandrea and A. Zunger, Phys. Rev. B **43**, 8962 (1991).
[11] P. Lavallard, C. Gourdon, and R. Planel, Superlattices Microstruct. **12**, 321 (1992).
[12] F. Fuchs, J. Schmitz, J.D. Rulston, P. Koidl, R. Hertz, and A. Hoffmann, Superlattices Microstruct. **16**, 35 (1994).
[13] O. Krebs and P. Voisin, Phys. Rev. Lett. **77**, 1829 (1996); O. Krebs, W. Seidel, J.P. Andre, D. Bertho, C. Jouanin, and P. Voisin, Semicond. Sci. Technol. **12**, 938 (1997).
[14] R. Magri and S. Ossicini, Phys. Rev. B **58**, R1742 (1998).
[15] S.B. Zhang and A. Zunger, Appl. Phys. Lett. **63**, 1399 (1993).
[16] J. Kim, L.W. Wang, and A. Zunger, Phys. Rev. B **57**, R9408 (1998).
[17] R.G. Dandrea, C.B. Duke, and A. Zunger, J. Vac. Sci. Technol. B **10**, 1744 (1992).
[18] C. Jenner, E. Corbin, B.M. Adderley, and M. Jaros, Semicond. Sci. Technol. **13**, 359 (1998).
[19] B.R. Bennett, B.V. Shanabrook, R.J. Wagner, J.L. Davis, J.R. Waterman, and M.E. Twigg, Solid-State Electron. **37**, 733 (1994).
[20] L.-W. Wang and A. Zunger, in *Semiconductor Nanoclusters*, Studies in Surface Science and Catalysis Vol. 103, edited by P.V. Kamat and D. Meisel (Elsevier Science, New York, 1996), p. 161.
[21] P. Keating, Phys. Rev. **145**, 637 (1966).
[22] L.W. Wang and A. Zunger, Phys. Rev. B **51**, 17 398 (1995).
[23] L.W. Wang, J. Kim, and A. Zunger, Phys. Rev. B **59**, 5678 (1999).
[24] M. Cohen and V. Heine, in *Solid State Physics*, edited by H. Ehrenreich, F. Seitz, and D. Turnbull (Academic Press, New York, 1970), Vol. 24, p. 64.
[25] L.-W. Wang and A. Zunger, Phys. Rev. B **51**, 17 398 (1995).
[26] S.-H. Wei and A. Zunger, Appl. Phys. Lett. **72**, 2011 (1998).
[27] C.G. Van de Walle, Phys. Rev. B **39**, 1871 (1989).
[28] Many previous $\mathbf{k}\cdot\mathbf{p}$ studies (Ref. 29) have drawn the deformation potentials of the VBM (a_v) from the ''model solid theory'' of Van de Walle (Ref. 27). However, more accurate LDA calculations [S.-H. Wei and A. Zunger, Phys. Rev. B (to be published)] show that due to cation *d* and anion *p* coupling, a_v are *negative* for Ga and In compounds, i.e., $a_v=-0.58,\ -1.21,\ -1.32,\ -0.41,\ -1.00,\ -1.24$ eV for GaP, GaAs, GaSb, InP, InAs, InSb, respectively, meaning that as volume is compressed, the VBM energy moves upwards. In contrast, the ''model solid theory'' neglects implicit $p-d$ coupling, thus, we find $a_v=+1.70,\ +1.16,\ +0.79,\ +1.27,\ +1.00$, 0.36 eV for GaP, GaAs, GaSb, InP, InAs, InSb, respectively.
[29] M.P.C.M Krijn, Semicond. Sci. Technol. **6**, 27 (1991).
[30] G.A. Sai-Halasz, Solid State Commun. **27**, 935 (1978).
[31] R. Kaspi *et al.* (private communication).
[32] L.L. Chang, G.A. Sai-Halasz, L. Esaki, and R. L. Aggarwal, J. Vac. Sci. Technol. **19**, 589 (1981).
[33] M.J. Yang and B.R. Bennett, Electron. Lett. **30**, 1710 (1994).
[34] D.H. Chow *et al.*, Appl. Phys. Lett. **56**, 1418 (1990).
[35] F. Fuchs, J. Schmitz, N. Herres, J. Wagner, J.D. Ralston, and P. Koidl, Inst. Phys. Conf. Ser. **144**, 219 (1995).
[36] D.K. Arch, G. Wicks, and T. Tonaue, J. Appl. Phys. **58**, 3933 (1985).
[37] A.Y. Lew, S.L. Zuo, E.T. Yu, and R.H. Miles, Phys. Rev. B **57**, 6534 (1998).
[38] M.E. Twigg, B.R. Bennett, and R. Magno, J. Cryst. Growth **191**, 651 (1998). Composition modulation has been shown to reduce dramatically the band gap in other III-V alloys; see, for example, T. Mattila, L. Bellaiche, L.-W. Wang, and A. Zunger, Appl. Phys. Lett. **72**, 2144 (1998).
[39] M.E. Twigg, B.R. Bennett, P.M. Thibado, B.V. Shanabrook, and L.J. Whitman, Philos. Mag. A **7**, 7 (1998).
[40] H. Mohseni *et al.*, Appl. Phys. Lett. **71**, 1403 (1997).